

Spin—orbit stable dirac nodal line in monolayer B_6O

Wen-Rong Liu(刘文荣), Liang Zhang(张亮), Xiao-Jing Dong(董晓晶), Wei-Xiao Ji(纪维霄), Pei-Ji Wang(王培吉), and Chang-Wen Zhang(张昌文)

Citation: Chin. Phys. B, 2022, 31 (**3**): 037305. DOI: 10.1088/1674-1056/ac4cba
Journal homepage: http://cpb.iphy.ac.cn; http://iopscience.iop.org/cpb

What follows is a list of articles you may be interested in

First principles study on geometric and electronic properties of two-dimensional Nb_2CT_x MXenes

Guoliang Xu(徐国亮), Jing Wang(王晶), Xilin Zhang(张喜林), and Zongxian Yang(杨宗献)
Chin. Phys. B, 2022, 31 (**3**): 037304. DOI: 10.1088/1674-1056/ac322e

Abnormal phenomenon of source-drain current of AlGaN/GaN heterostructure device under UV/visible light irradiation

Yue-Bo Liu(柳月波), Jun-Yu Shen(沈俊宇), Jie-Ying Xing(邢洁莹), Wan-Qing Yao(姚婉青), Hong-Hui Liu(刘红辉), Ya-Qiong Dai(戴雅琼), Long-Kun Yang(杨隆坤), Feng-Ge Wang(王风格), Yuan Ren(任远), Min-Jie Zhang(张敏杰), Zhi-Sheng Wu(吴志盛), Yang Liu(刘扬), and Bai-Jun Zhang(张佰君)
Chin. Phys. B, 2021, 30 (**11**): 117302. DOI: 10.1088/1674-1056/abfa07

Edge states enhanced by long-range hopping: An analytical study

Huiping Wang(王会平), Li Ren(任莉), Liguo Qin(秦立国), and Yueyin Qiu(邱岳寅)
Chin. Phys. B, 2021, 30 (**10**): 107301. DOI: 10.1088/1674-1056/abe9a5

Signatures of strong interlayer coupling in γ-InSe revealed by local differential conductivity

Xiaoshuai Fu(富晓帅), Li Liu(刘丽), Li Zhang(张力), Qilong Wu(吴奇龙), Yu Xia(夏雨), Lijie Zhang(张利杰), Yuan Tian(田园), Long-Jing Yin(殷隆晶), and Zhihui Qin(秦志辉)
Chin. Phys. B, 2021, 30 (**8**): 087306. DOI: 10.1088/1674-1056/abff32

Band alignment of p-type oxide/ε-Ga_2O_3 heterojunctions investigated by x-ray photoelectron spectroscopy

Chang Rao(饶畅), Zeyuan Fei(费泽元), Weiqu Chen(陈伟驱), Zimin Chen(陈梓敏), Xing Lu(卢星), Gang Wang(王钢), Xinzhong Wang(王新中), Jun Liang(梁军), Yanli Pei(裴艳丽)
Chin. Phys. B, 2020, 29 (**9**): 097303. DOI: 10.1088/1674-1056/ab9c0d

---

Spin–orbit stable dirac nodal line in monolayer B_6O

Wen-Rong Liu(刘文荣)[1], Liang Zhang(张亮)[1], Xiao-Jing Dong(董晓晶)[2], Wei-Xiao Ji(纪维霄)[1], Pei-Ji Wang(王培吉)[1], and Chang-Wen Zhang(张昌文)[1,†]

[1] *School of Physics and Technology, Institute of Spintronics, University of Jinan, Jinan* 250022, *China*
[2] *School of Physics and Physical Engineering, Qufu Normal University, Qufu* 273100, *China*

(Received 17 September 2021; revised manuscript received 3 January 2022; accepted manuscript online 19 January 2022)

The two-dimensional (2D) materials with nodal line band crossing have been attracting great research interest. However, it remains a challenge to find high-stable nodal line structure in 2D systems. Herein, based on the first-principles calculations and theoretical analysis, we propose that monolayer B_6O possesses symmetry protected Dirac nodal line (DNL) state, with its Fermi velocity of 10^6 m/s in the same order of magnitude as that of graphene. The origin of DNL fermions is induced by coexistence of time-reversal symmetry and inversion symmetry. A two-band tight-binding model is further given to understand the mechanism of DNL. Considering its robustness against spin–orbit coupling (SOC) and high structural stability, these results suggest monolayer B_6O as a new platform for realizing future high-speed low-dissipation devices.

Keywords: monolayer B_6O, Dirac nodal line, two-band tight-binding model

PACS: 73.20.At, 75.70.Ak, 75.70.Cn **DOI:** 10.1088/1674-1056/ac4cba

The 2D materials[1–4] have attracted much attention because of their rich properties. Among the rest, topological semimetals (TSMs) are a class of systems in which the conduction and valence bands cross each other within the Brillouin zone, while they are robust. These excellent properties provide a unique site for singular phenomena derived from band topology.[5,6] DNL semimetals,[7–19] as one of the TSMs, connect the gapless and gapped phases and can be tuned to a variety of other topological phases, such as topological insulators, Dirac and Weyl semimetals.[20–27] It has become a new class of quantum materials that are more promising for scientific research. Many excellent physical properties have been obtained in these nodal line materials, including Friedel oscillation, nondispersive Landau energy level,[28] and specific long-range Coulomb interactions,[29] etc., which pioneers a new path for Dirac materials in future low dissipation device applications. These proposals, however, are dependent on the effect of spin–orbit coupling (SOC): when SOC is considered, the structure of node line will be broken, and there is a sizable gap at the intersection of conduction band and valence band. Until now, $PbTaSe_2$, a nodal line semi-metallic structure with strong SOC, is only experimentally confirmed.[12]

The fundamental conceptions of Dirac, Weyl and DNL semimetals are also suitable for use in 2D materials. Some current theoretical works.[30–32] illustrate nodal wire-band crossing with weak SOC. However, similar to the three-dimensional (3D) case, the nodal line band present in these materials is broken when SOC is turned on. It is reported that 2D DNL fermions with SOC in single-layer Cu_2Si have been realized experimentally.[33] Interestingly, a recent article[34] summarizes and classifies all possible structures with cross properties in 2D noncentro-symmetric systems with SOC and time inversion invariance. According to the prediction of this research, when a material has appropriate geometric symmetry, the node line band crossing is stable for SOC. In fact, weak SOC materials, such as Be_2C, BeH_2,[35] and Na_2CrBi trilayer[36] are proposed as intriguing 2D nodal line materials. Therefore, finding 2D materials with high-stable nodal line bands is a more nontrivial work.

In this paper, we demonstrate that monolayer B_6O (Figs. 1(a) and 1(b)), which has remarkably energetic stability and positively dynamical stability, possesses a nodal line band structure that maintains robust even if considering the effect of SOC. Compared with the single Dirac point of other 2D allotropes, the band structure of B_6O is characterized by elliptical DNL, and its Fermi velocity is 10^6 m/s, which is as the same as that of graphene. The nodal line band crossing is further explained by combining $\boldsymbol{k}\cdot\boldsymbol{p}$ model calculation with symmetry analysis. Also, B_6O/h-BN superstructure is proposed to realize DNL feature of monolayer B_6O in experiments. Our results not only reveal a new DNL fermion of matter, but also offer promising material platform for realizing novel low-dissipation devices.

All the structural and electronic properties are calculated by using the projector augmented wave (PAW) method[37] implemented in the Vienna *ab initio* simulation package (VASP) code.[38,39] The Perdew–Burke–Ernzerhof (PBE) form of the generalized gradient approximation (GGA) exchange–correlation functional[40] is adopted, while the more accurate electronic band structure is obtained by HSE06[41,42] hybrid functional. The wave functions of all systems are expanded by using a plane wave basis with a cut-off energy of 550 eV,

†Corresponding author. E-mail: ss_zhangchw@ujn.edu.cn
© 2022 Chinese Physical Society and IOP Publishing Ltd

and the Brillouin zone sampling grids are set to be concentrated enough to guarantee convergence. The maximum force is less than 0.01 eV/Å during optimization. The vibrational spectrums are simulated by using DFT perturbation theory as implemented in the PHONOPY code.[43] The 3D energy band structure of monolayer B_6O is obtained from the post-processing maximum localized Wannier Hamiltonian derived from the code of WANNIER90.[44–46]

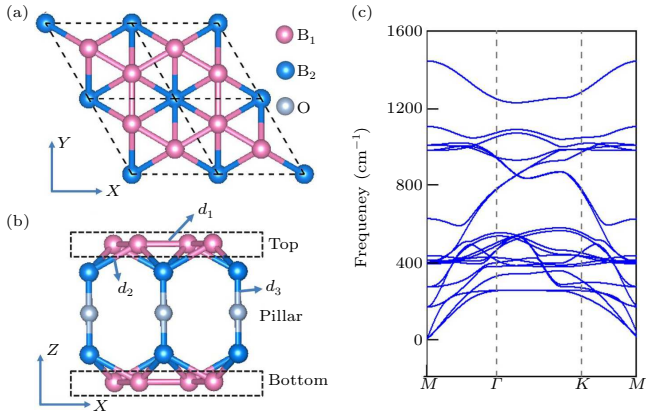


Fig. 1. (a) and (b) The top and side views of monolayer B_6O with lattice vectors a ($\sim$ 2.88 Å) in the x–y plane. The unit cell is marked with a rhombus. (c) The phonon spectrum of B_6O.

Monolayer B_6O has a hexagonal configuration with three different types of atoms in a unit cell and shares the space group *P6/mmm* symmetry, as illustrated in Fig. 1(a). The outmost-layer B_1 atoms possess graphenelike plane, while the second kind B_2, accompanied with oxygen, banked up between top and bottom B_1 planes, forms a pillar that hold two B_1 layers. There are three kinds of bond lengths, which are labeled d_1, d_2, and d_3, as shown in Fig. 1(b). The $d_1 = 1.66$ Å is the length of the outmost graphene-like layered bonding, which is formed by two B_1 atoms close to sp^2 hybridization and the value of d_1 is close to that of graphene. All the other B_2 atoms form a bond length, $d_2 = 1.91$ Å, while $d_3 = 1.36$ Å is along for B_2–O–B_2 pillar. The chemical bonding character of B_6O can be illustrated by the electron localization function (ELF) in Fig. 2. One can see that ELF is situated on the area in the middle of the B_1–B_1 bonds within the flat hexagonal plane (Fig. 2(a)), whereas no electron localization occurs in between B_1–B_2 atoms (Fig. 2(b)), suggesting the ionic bond character along B–O bonding. Similar results are found for B_2–O–B_2 bonding. Additionally, the ELF plots for the sliced planes are shown in Figs. 2(d)–2(f), where a high ELF distribution (0.75) is centered at the middle of B_1–B_1 and B_2–O–B_2 bonding, suggesting a very strong covalent bond. While for the sliced plane in Fig. 2(e), the ELF equals to 0.4, suggesting partially ionic bond, which is consistent with the Bader charge analysis.[47] Further calculation and analysis show that the column composed of B_2–O–B_2 has an average of 0.85 electrons transferred to its adjacent B_1, i.e., B_2 atoms act as an electron supply source to transfer electrons to the unoccupied state of sp^2 in plane, so that the stability of B_6O is significantly enhanced. This mechanism is similar to the boronrich borides MB_2 or MB_4, where B atoms form a hexagonal lattice like to graphene and interact with triangular metal lattice.[48] Therefore monolayer B_6O is ionic, consisting of graphenelike plane and B_2O pillars.

Structural stability of B_6O can be further evaluated by the formation energy as $E_{coh} = E_{B_6O} - 6E_B - 1/2E_{O_2}$, where E_{B_6O} is the total energy of B_6O, E_B and E_{O_2} is the energy of B atom and oxygen, respectively. The relative energy is –5.13 eV/atom, which is close to that of other boron-based allotropes such as B_2S_3 (–4.9 eV/atom)[49] and B_2S (–5.3 eV/atom).[50] The dynamical stability of B_6O is also checked from the vibrational spectrum, as shown in Fig. 1(c). There is no appreciable imaginary frequency in the phonon energy spectrum, establishing the dynamically structural stability of B_6O. That is to say, when the lattice vibration is normal, B_6O can maintain its basic crystal structure. We also calculate the elastic constants and find that C_{11}, C_{12}, C_{22}, and C_{66} are 236.02 N/m, 231.25 N/m, 231.28 N/m, and 104.76 N/m, respectively. These values content the mechanical stability criteria ($C_{11} \times C_{22} - C_{22}^2 > 0$, $C_{66} > 0$), which illustrates that B_6O has good mechanical stability and can resist small deformation. Through *ab initio* molecular dynamics simulation, after heating to 300 K in a time step of 1 fs, B_6O still maintains its basic crystal structure, small thermal oscillation and no obvious structural collapse. All these results illustrate that monolayer B_6O has excellent thermostability and can retain its structural integrity at room temperature.

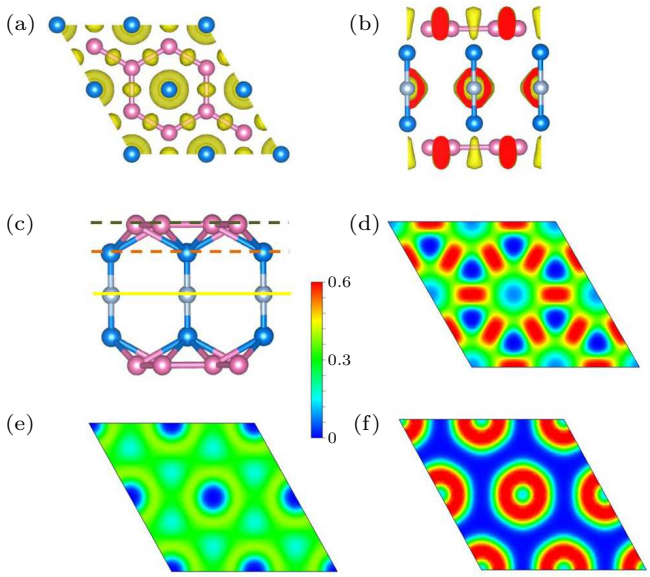


Fig. 2. (a) Top view and (b) side view of the electron localization function of monolayer B_6O with isovalue 0.8. (c) The different cutting planes for ELF. The ELF of plane cut along the olive dotted line (d), along the orange dotted line (e) and along the yellow solid line (f).

Figure 3(a) presents the band structure along the M–Γ–K–M path for monolayer B_6O. It portrays the nodal line band structure, and although SOC is considered, the energy band

structure remains stable due to its $\hat{M}_Z$ specular reflection symmetry (Fig. 1(b)). Interestingly, the bottom of conduction band and the top of valence band cross near the K point and form a typical DNL. In order to confirm whether single-layer B_6O is a real node line crossing or an anti-crossing structure with small energy separation, we use a theoretical model mentioned in recent research[34] to classify the band crossings in 2D systems. According to the theoretical analysis, if (i) the 2D plane has mirror reflection symmetry, and (ii) the two crossed bands have different mirror eigenvalues, it can be explained that the nodal semi-metallic state of 2D material will be stable.

For monolayer B_6O in Fig. 1(a), it is unchangeable under the mirror reflection about x–y plane, so it meets the situation described in condition (i). In this respect, the Hamiltonian $\hat{H}$ should commute with the mirror reflection operator $\hat{M}_Z$

$$\left[\hat{H}, \hat{M}_Z\right] = 0. \tag{1}$$

Obviously, $\hat{M}_Z$ does not change the 2D momentum k, demonstrating that the energy eigenstates for the crystal momentum k are eigenstates of $\hat{M}_Z$. Due to the eigenvalue spectrum of $\hat{M}_Z$ is discrete, the continuous change of energy eigenstates as a function of k in an energy band cannot change the eigenvalue of $\hat{M}_Z$, so each energy band of $\hat{H}$ has a well-defined mirror eigenvalue.

We now take the mirror eigenvalues of DNL into account, which attracts our interest. As can be seen from Fig. 3, there are two crossing bands interacting along the high symmetry Γ–K–M line in momentum space. Contributions of different orbits are represented by the orbital-projected density of states (DOSs). Two bands close to E_F originate from the B-p_z orbital, linearly crossing each other, then the charge carriers can be characterized by massless Dirac fermions. This is similar to the most other 2D lattices with a Dirac point, such as Mn-DCA,[51] while the p_x/p_y atomic orbitals only play a role in the energy bands. Obviously, when there is no symmetry protection, the two cross energy bands will interact which results in opening of the band gap. In order to check whether the two bands meet condition (ii), rough information of the wave function characteristics of the two bands is required, because the mirror eigenvalues may be discontinuous, and the mirror eigenvalues of each band can be determined to the wave functions. In the reciprocal space of $P6/mmm$, high-symmetry line Γ–K possess a little D_{3h} point group, including a twofold rotation axe C_{2y} and threefold rotation axe C_{3z}. In this respect, the K point is just the time-reversal-symmetry (T) partner in momentum space. The algebraic relationship within these generators should be written as

$$[C_{3z}, M_z] = 0, \quad [C_{2y}, M_z] = 0, \quad C_{3z}C_{2y} = C_{21}C_{3z}, \tag{2}$$

$$C_{3z}^3 = M_z^2 = C_{2y}^2 = 1. \tag{3}$$

Here, the occupied and unoccupied low-energy bands at K point are doubly degenerate. Making use of D_{3h} group analysis, we find that irreducible representations (IRs) of p_z band near K point are E' and E'', respectively. According to Eqs. (1)–(3), the whole BZ is invariant for $\hat{M}_Z$ and at any K points, the eigenvalues of C_{3z} and C_{2y} of all bands keep their signs unchanged. Since the IRs E' and E'' do not couple with each other, a DNL forms centered K point, which will be discussed further with a theoretical $\boldsymbol{k}\cdot\boldsymbol{p}$ model later.

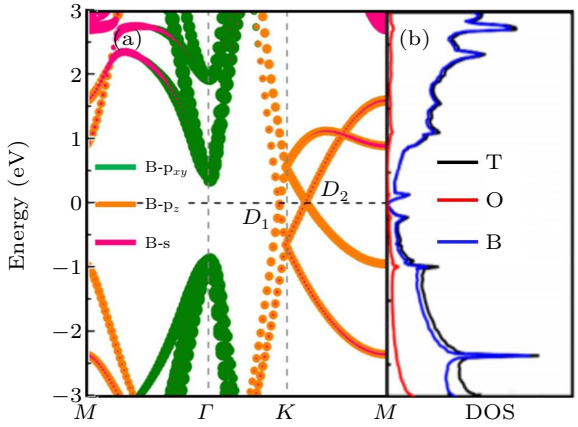


Fig. 3. (a) Orbital projected band structure of B_6O. The orbital contribution is drawn in different colors, and the spot size represents its weight. The green, yellow and purple dots denoted the p_{xy}, p_z, and s orbitals of boron, respectively. (b) Density of states, where the blue, red and black lines represent the contributions of B atoms, O atoms and the total contribution, respectively.

To confirm this expectation of B_6O, we propose 3D band dispersion based on B-p orbit by constructing tight bound Hamiltonian from MLWFs.[52] Figure 4(a) displays the calculated MLWF and DFT band structures, which in perfect agreement with DFT results, further confirming the accuracy of our B_6O orbital component analysis. As a consequence, an entire elliptical DNL centered at K point can be obtained, see Fig. 4(b). It is clearly different from conventional Dirac-cone materials with a discrete DP near E_F. In order to visually display the band touching, we further perform a scan around crossing point D_1 along Γ–K direction. The linearly dispersed B-p_z band crosses each other, forming a serial of DPs with a tip to tip. Similar results are observed for K–M direction for B_6O. Noticeably, though 3D DNL state has been observed experimentally, DNL in 2D boron-based sheet is rarely reported. The intriguing point of B_6O band structure is that the band crossings in MS form a closed DNL because of the coexistence of time reversal and inversion symmetry.

From the crossing point with linear bands of B_6O, we estimate the Fermi velocity (v_F), by a linear fitting of DFT results. v_F can be understood as the transmission velocity of massless Dirac fermions, and the calculation formula is expressed as

$$v_F = \frac{1}{\hbar}\frac{\partial E}{\partial k}. \tag{4}$$

Here, the v_F after unit conversion is expressed as

$$v_F = \frac{\mathrm{d}E}{\mathrm{d}k} = \frac{\Delta E \times 1.6 \times 10^{-19} \times a \times 10^{-10}}{\frac{\Delta k}{k_t} \times \frac{4\pi}{3} \times 1.0545 \times 10^{-34}}, \tag{5}$$

where k_t is the total number of points from Γ to M, Δk is the number of K points on a certain energy band taken between Γ to M, ΔE is the energy difference of this energy band, and a is the lattice constant of structure.

We find that the radial velocities of the Dirac point are in the range of 0.54×10^6–0.63×10^6 m/s, which is comparable to the value 0.82×10^6 m/s in graphene. It is the ultrahigh Fermi velocity of B_6O that is advantageous for building high-speed electronic devices such as field effect transistor.

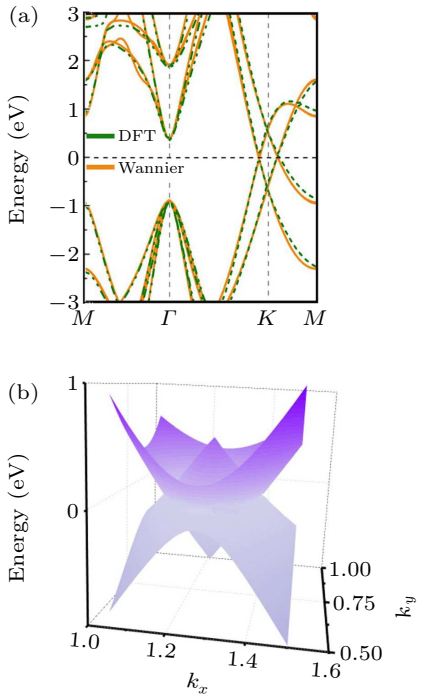


Fig. 4. (a) Comparison of the band structures obtained by DFT (green) and Wannier (purple) simulations. (b) The 3D energy bands of monolayer B_6O.

Now, we discuss the forming mechanism of DNL by inferring an effective low-energy $\boldsymbol{k}\cdot\boldsymbol{p}$ model. As a general rule, a two-band Hamiltonian capturing the band crossing is able to be written as

$$H(k) = \sum_{i=0}^{3} d_i(k)\sigma_i, \tag{6}$$

where $d_i(k)$, $(i = 1, 2, 3)$ is real function of $k(k_x, k_y, k_z)$. σ_0 and $\sigma_{1,2,3}$ are the 2×2 unit matrix and Pauli matrices characterizing the space of two bands, which are mainly from B-p orbitals in B_6O. In the space group $P6/mmm$, the k is not an invariant point under P or T, but the TP symmetry keeps the K point invariant, and it commutes with all generators. So we can write down $PT = \kappa$, where κ is the complex conjugation in a proper orbital basis. Here, the spin and orbital part of the electronic wave function are decoupled. Therefore, for each spin channel, all crystalline symmetries are retained separately as for non-spin particles. By the symmetry analysis, the two crossing bands in $k_z = 0$ plane have opposite eigenvalues of M_z. Along the ΓK direction, these two bands with the same eigenvalues of C_{2y} and opposite eigenvalues of M_x. Thus, the representation matrices of these generators requires that

$$C_{2y} = \sigma_0,\ \ M_z = \sigma_z,\ \ M_x = \sigma_z,\ \ PT = \kappa. \tag{7}$$

According to

$$C_n H(\boldsymbol{k}) C_n^{-1} = H(C_n \boldsymbol{k}), \tag{8}$$

we can obtain

$$C_{2y} H(k_x, k_y, k_z) C_{2y}^{-1} = H(-k_x, k_y, -k_z), \tag{9}$$

$$M_z H(k_x, k_y, k_z) M_z^{-1} = H(k_x, k_y, -k_z), \tag{10}$$

$$(PT) H(k_x, k_y, k_z) (PT)^{-1} = H^*(k_x, k_y, k_z) = H(k_x, k_y, k_z). \tag{11}$$

Considering that

$$[C_{3z}, M_z] = 0 \ \text{ and } \ M_z = \sigma_z, \tag{12}$$

$d_3(k)$ can be further constraint as

$$d_3(k_+, k_-, k_z) = d_3\left(e^{i2\pi/3} k_+, e^{-i2\pi/3} k_-, k_z\right). \tag{13}$$

Finally, at the $k_z = 0$ plane, to the second order of k, we can infer that

$$d_1(k) = 0,\ \ d_2(k) = 0, \tag{14}$$

$$d_3(k) = M - A\left(k_x^2 + k_y^2\right). \tag{15}$$

Thus, B_6O forms a DNL when $M/A > 0$.

The effects of HSE06 on band structure of B_6O are further examined. We find that the band structures along Γ–K–M line at HSE06 level are similar to that of PBE level, where two crossing bands linearly remains at E_F. Although the PBE underestimates the band gap at Γ point, the fact that HSE06 method gives the same DNL strengthens our understanding of the effectiveness of B_6O band structure, which presents an ideal material for practical applications. In 2016, Fang *et al.*[53] reviewed the theoretical research progress of nodal line semimetals, in which the explicit form of topological invariants of each symmetric group is discussed by analyzing the wave function on Fermi surface. Zhang *et al.*[54] also found that the formation mechanism of $Tl_2Nb_2O_{6.5}$ triply-degenerate nodal point can be well explained by $\boldsymbol{k}\cdot\boldsymbol{p}$ model. We believe our work can further promote the progress of research on DNL in 2D materials.

Now, we consider the stability of the nodal line band in the case of symmetry breaking. When we break the C_3 rotational symmetry, the nodal line is still robust owing to the M_z mirror symmetry. On the contrary, when we break the M_z mirror symmetry, the node lines not any more exist stably and may evolve into Dirac points or anti crossing structures. If some points on the nodal line become vestigial owing to the

residual symmetry after the destruction of M_z mirror symmetry, the nodal line structure turns into Dirac points. In this case, B_6O has M_x mirror symmetry, which can guarantee the degeneracy on the M_x mirror invariant line. However, as shown in Fig. 1(b), the K (K') point is not on the M_x mirror symmetry line along the Γ–M line in the momentum space, so the nodal line energy band crossing becomes a Dirac point band structure.

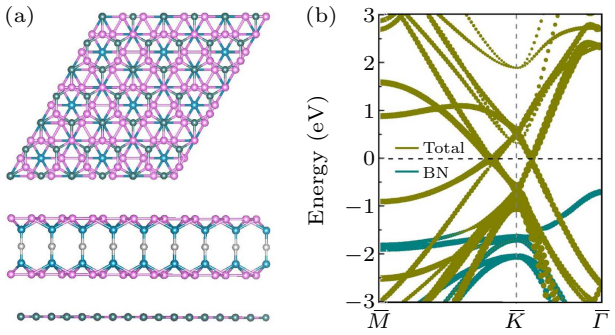


Fig. 5. (a) Top and side view of the epitaxial growth of B_6O on h-BN substrate. (b) The corresponding energy band structure without SOC. The green and blue green dots are mainly from B_6O and h-BN, respectively.

It is inevitable that the 2D lattice grows on the substrate, which will break the spatial symmetry of B_6O, resulting in a gap in the energy bands of DNL. However, the Dirac points can be maximally preserved due to the weak interface interactions in between two sublattices. For instance, ARPES measurements do not give any characteristics about the gap opening of NL dispersion in 2D Cu_2Si.[33] From the perspective of practical applications, the inherited quantum transport in Dirac materials is more fascinating because it is less vulnerable to symmetry breaking. As a matter of fact, Dirac point resides only in a free-standing graphene owing to symmetry protection. When graphene is deposited on substrate, the spatial symmetry of the two carbon atoms is broken, which leads to the opening of the gap in graphene. However, the quantum transport which is in graphene, including half-integer quantum Hall effect,[55,56] fractional QHE,[57] and ultra-high carrier mobility,[58] remains in graphene deposited on multifarious substrates. Consequently, we deduce that the quantum properties of NL materials can be maintained in B_6O-based heterostructure (HTS) so long as the space symmetry is preserved to a large extent. To confirm this, we put B_6O on h-BN substrate to construct B_6O/h-BN HTS, which is illustrated in Fig. 5(a). Structural optimizations demonstrate that the layer spacing between B_6O and h-BN substrate is 3.18 Å with a weaker binding energy of 34.6 meV, indicating the existence of van der Waals interaction. Figure 5(b) shows the band structure of B_6O/h-BN in the energy range of -3 eV to 3 eV, in consistent with that of monolayer B_6O. Also, the DNL fermions around K point keep well, only a tiny band gaps (a few 0.23 meV) are opened due to the symmetrical characteristic broken.

In summary, we predicted the DNL phase in 2D B_6O allotrope based on first-principles calculations and TB model, which has an outstanding energetic stability and superior dynamical stability. It possesses an elliptical DNL fermion, with a Fermi velocity of 10^6 m/s perfectly matched the order of magnitude of graphene. A two-band $\boldsymbol{k}\cdot\boldsymbol{p}$ model is constructed to explain the formation mechanism of DNL in B_6O. It is worth mentioning that Anosha Rubab *et al.*[59] reported that borophene is a perfect Dirac material. Its large surface area, high Young's modulus and extremely high Fermi velocity make it applicable to sensors, electronics and energy converters. In 2019, Zuo *et al.*[60] also found that time reversal symmetry and mirror reflection symmetry can protect the nodal line in β-boron sheet, and a nanodevice that can manipulate and control the nodal line has been proposed. These findings have opened up a new path for the realization of novel high-speed and low-power devices, and 2D B_6O may be a new platform for the development of nano-devices in the future.

Acknowledgments

Project supported by Taishan Scholar Program of Shandong Province, China (Grant No. ts20190939), Independent Cultivation Program of Innovation Team of Jinan City (Grant No. 2021GXRC043), and the National Natural Science Foundation of China (Grant Nos. 52173283 and 62071200).

References

[1] Jiang F X, Zhao Y, Zhou G W, Zhang J, Fan J P and Xu X H 2015 *Chin. Phys. Lett.* **32** 087501
[2] Pan L, Wen H, Huang L, Chen L, Deng H X, Xia J B and Wei Z 2019 *Chin. Phys. B* **28** 107504
[3] Zhang S S, Ji W X, Zhang C W, Zhang S F, Li P, Li S S and Yan S S 2018 *Chin. Phys. Lett.* **35** 087303
[4] Zhang S J, Zhang C W, Zhang S F, Ji W X, Wang P J, Li S S and Yan S S 2017 *Phys. Rev. B* **96** 205433
[5] Armitage N P, Mele E J and Vishwanath A 2018 *Rev. Mod. Phys.* **90** 15001
[6] Kim Y, Wieder B J, Kane C L and Rappe A M 2015 *Phys. Rev. Lett.* **115** 036806
[7] Mullen K, Uchoa B and Glatzhofer D T 2015 *Phys. Rev. Lett.* **115** 026403
[8] Yu R, Weng H, Fang Z, Dai X and Hu X 2015 *Phys. Rev. Lett.* **115** 036807
[9] Fu B, Fan X, Ma D, Liu C C and Yao Y 2018 *Phys. Rev. B* **98** 1
[10] Feng X, Yue C, Song Z, Wu Q and Wen B 2018 *Phys. Rev. Mater.* **2** 014202
[11] Wang J T, Nie S, Weng H, Kawazoe Y and Chen C 2018 *Phys. Rev. Lett.* **120** 26402
[12] Bian G, Chang T R and Sankar R 2016 *Nat. Commun.* **7** 10556
[13] Hu J, Tang Z, Liu J, Liu X, Zhu Y, Graf D, Myhro K, Tran S, Lau C N, Wei J and Mao Z 2016 *Phys. Rev. Lett.* **117** 016602
[14] Li R, Ma H, Cheng X, Wang S, Li D, Zhang Z, Li Y and Chen X Q 2016 *Phys. Rev. Lett.* **117** 096401
[15] Kobayashi S, Yamakawa Y, Yamakage A, Inohara T, Okamoto Y and Tanaka Y 2017 *Phys. Rev. B* **95** 1
[16] Zhang R W, Liu C C, Ma D S, Wang M and Yao Y 2018 *Phys. Rev. B* **98** 1
[17] Bzdušek T, Wu Q S, Rüegg A, Sigrist M and Soluyanov A A 2016 *Nature* **538** 75

[18] Wang S S, Liu Y, Yu Z M, Sheng X L and Yang S A 2017 *Nat. Commun.* **8** 1
[19] Yan Z, Bi R, Shen H, Lu L, Zhang S C and Wang Z 2017 *Phys. Rev. B* **96** 1
[20] Andrei Bernevig B, Taylor L and Hughes S C Z 1998 *Science* **314** 1757
[21] Wan X, Turner A M, Vishwanath A and Savrasov S Y 2011 *Phys. Rev. B* **83** 1
[22] Yang B J and Nagaosa N 2014 *Nat. Commun.* **5** 4898
[23] Wang Z, Sun Y, Chen X Q, Franchini C, Xu G, Weng H, Dai X and Fang Z 2012 *Phys. Rev. B* **85** 1
[24] Zhang M H, Zhang C W, Wang P J and Li S S 2018 *Nanoscale* **10** 20226
[25] Weng H, Fang C, Fang Z, Andrei Bernevig B and Dai X 2015 *Phys. Rev. X* **5** 011029
[26] Soluyanov A A, Gresch D, Wang Z, Wu Q, Troyer M, Dai X and Bernevig B A 2015 *Nature* **527** 495
[27] Li S S, Ji W X, Hu S J, Zhang C W and Yan S S 2017 *ACS Appl. Mater. Inter.* **9** 41443
[28] Rhim J W and Kim Y B 2015 *Phys. Rev. B* **92** 1
[29] Huh Y, Moon E G and Kim Y B 2016 *Phys. Rev. B* **93** 1
[30] Lu J L, Luo W, Li X Y, Yang S Q, Cao J X, Gong X G and Xiang H J 2017 *Chin. Phys. Lett.* **34** 057302
[31] Jin Y J, Wang R, Zhao J Z, Du Y P, Zheng C Di, Gan L Y, Liu J F, Xu H and Tong S Y 2017 *Nanoscale* **9** 13112
[32] Zhou P, Ma Z S and Sun L Z 2018 *J. Mater. Chem. C* **6** 1206
[33] Feng B, Fu B and Kasamatsu S 2017 *Nat. Commun.* **8** 8
[34] Park S and Yang B J 2017 *Phys. Rev. B* **96** 1
[35] Yang B, Zhang X and Zhao M 2017 *Nanoscale* **9** 8740
[36] Niu C, Buh P M, Zhang H, Bihlmayer G, Wortmann D, Blögel S and Mokrousov Y 2017 arXiv:1703.05540
[37] Blöchl P E 1994 *Phys. Rev. B* **50** 17953
[38] Kresse G J F 1996 *Phys. Rev. B* **54** 11169
[39] Kresse G and Joubert D 1999 *Phys. Rev. B* **59** 1758
[40] Perdew J P, Burke K and Ernzerhof M 1996 *Phys. Rev. Lett.* **77** 3865
[41] Heyd J, Scuseria G E and Ernzerhof M 2003 *J. Chem. Phys.* **118** 8207
[42] Paier J, Marsman M, Hummer K, Kresse G, Gerber I C and Angyán J G 2006 *J. Chem. Phys.* **124** 154709
[43] Togo A and Tanaka I 2015 *Scr. Mater.* **108** 1
[44] Mostofi A A, Yates J R, Lee Y S, Souza I, Vanderbilt D and Marzari N 2008 *Comput. Phys. Commun.* **178** 685
[45] Lopez Sancho M P, Lopez Sancho J M and Rubio J 1984 *J. Phys. F Met. Phys.* **14** 1205
[46] Wu Q S, Zhang S N, Song H F, Troyer M and Soluyanov A A 2018 *Comput. Phys. Commun.* **224** 405
[47] Henkelman G, Arnaldsson A and Jónsson H 2006 *Comput. Mater. Sci.* **36** 354
[48] Alarco J A, Talbot P C and Mackinnon I D R 2015 *Phys. Chem. Chem. Phys.* **17** 25090
[49] Liu W, Miao M and Liu J Y 2015 *J. Mater. Chem. C* **3** 9921
[50] Zhao Y, Li X, Liu J, Zhang C and Wang Q 2018 *J. Phys. Chem. Lett.* **9** 1815
[51] Wang Y P, Ji W X, Zhang C W, Li P, Wang P J, Kong B, Li S S, Yan S S and Liang K 2017 *Appl. Phys. Lett.* **110** 233107
[52] Marzari N and Vanderbilt D 1997 *Phys. Rev. B* **56** 12847
[53] Fang C, Weng H, Dai X and Fang Z 2016 *Chin. Phys. B* **25** 117106
[54] Zhang W, Luo K, Chen Z, Zhu Z, Yu R, Fang C and Weng H 2019 *npj Comput. Mater.* **5** 1
[55] Novoselov K S, Geim A K, Morozov S V, Jiang D, Katsnelson M I, Grigorieva I V, Dubonos S V and Firsov A A 2005 *Nature* **438** 197
[56] Wang Y P, Ji W X, Zhang C W, Li P, Zhang S F, Wang P J, Li S S and Yan S S 2017 *Appl. Phys. Lett.* **110** 213101
[57] Dean C R, Young A F, Cadden-Zimansky P, Wang L, Ren H, Watanabe K, Taniguchi T, Kim P, Hone J and Shepard K L 2011 *Nat. Phys.* **7** 693
[58] Weiss N O, Zhou H, Liao L, Liu Y, Jiang S, Huang Y and Duan X 2012 *Adv. Mater.* **24** 5782
[59] Rubab A, Baig N, Sher M and Sohail M 2020 *Chem. Eng. J.* **401** 126109
[60] Zuo X, Dias A C, Liu F, Han L, Li H, Gao Q, Jiang X, Li D, Cui B, Liu D and Qu F 2019 *Phys. Rev. B* **100** 115423